LA-8524-PR

Progress Report

C.3

Applied Nuclear Data

Research and Development

April 1—June 30, 1980

LOS ALAMOS SCIENTIFIC LABORATORY

Post Office Box 1663   Los Alamos. New Mexico 87545

The four most recent reports in this series,
unclassified, are LA-8036-PR, LA-8157-PR,
LA-8298-PR, and LA-8418-PR.

This report was not edited by the Technical
Information staff.

Applied Nuclear Data

Research and Development

April 1—June 30, 1980

Compiled by

C. I. Baxman and P. G. Young

CONTENTS

APPLIED NUCLEAR DATA RESEARCH AND DEVELOPMENT
QUARTERLY PROGRESS REPORT
April 1 - June 30, 1980

Compiled by

C. I. Baxman and P. G. Young

ABSTRACT

This progress report describes the activities of the
Los Alamos Nuclear Data Group for the period April 1 through
June 30, 1980. The topical content is summarized in the Table
of Contents.

I. THEORY AND EVALUATION OF NUCLEAR CROSS SECTIONS

A. Non-Orthogonal Channels in R-Matrix Theory (G. M. Hale)

One of the traditional assumptions of R-matrix theory is that the two-body
channel functions upon which the wavefunction is projected at the channel sur-
face are orthogonal in the region external to the surface, even for different
arrangements. This assumption appears to hold for channel surfaces drawn at
radii close to the sizes of the clusters in systems having moderately large num-
bers of degrees of freedom, but one might expect it to break down in systems
(light nuclei) or for mechanisms (direct rearrangements) having few degrees of
freedom. We suspect that evidence for this breakdown is showing up in the ab-
normally large channel radii required in our R-matrix analysis of p-^{3}He and p-p
scattering, especially to fit the low-energy data.

We are studying this problem in the simplest and most extreme case, that of
three particles and two (two-body) arrangement channels. This configuation also
can be used to describe single-particle exchange contributions to reactions
among more than three particles. Using the notation $c_1 = (1,23)$ (particle 1
separated from a bound state of particle 2 and 3) and $c_3 = (3,12)$, one can see

that the reaction $c_1 \to c_3$ amounts to the transfer of particle 2. Even if one assumes that the internal eigenstates $|\lambda)$ of the system satisfying R-matrix boundary conditions are channel 1-type cluster states, they have non-zero projections $\gamma_{c_3\lambda} = (c_3|\lambda)$ on the channel 3 surface due to the non-orthogonality of c_1 and c_3. One obtains an expression of the form

$$\gamma_{c_3\lambda} = [\gamma_{c_1\lambda} I_1 (E_\lambda, B_3) + (c_3|V_3|\lambda)]/[1-I_3(E_\lambda,B_3)] \quad ,$$

where $\gamma_{c_1\lambda} = (c_1|\lambda)$ is the (presumed large) projection of $|\lambda)$ on the channel 1 surface and $-B_3$ is the energy of particles 1 and 2 bound in channel 3 by potential V_3. The integrals I_1 and I_3 are complicated, but they tend to be large as E_λ approaches the "exchange pole" energy

$$E_x = -\frac{1}{1-\alpha} B_3, \quad \alpha = \frac{m_1 m_3}{(m_1 + m_2)(m_1 + m_2)} \quad ,$$

and thus give $\gamma_{c_3\lambda} = -\gamma_{c_1\lambda}$ in the limit $E_\lambda \to E_x$.

B.   The ^{5}Li Compound Nucleus   (D. C. Dodder and G. M. Hale)

The ^{5}Li compound nucleus and its mirror twin ^{5}He are major objects of experimental studies because of their importance in practical energy-producing fusion processes as well as their intrinsic scientific interest. Because of the spins of the particles (d + ^{3}He in the case of ^{5}Li) most often used in the direct preparation of the compound nucleus, both the experimental programs and the theoretical interpretation of them are very complicated. The experimental apparatus is formidable, utilizing polarized particle beams and targets, while the theoretical analysis uses a complex R-matrix fitting code EDA developed at Los Alamos Scientific Laboratory (LASL) specifically for problems of this kind.

The scope of the problem is seen by considering the data base. There are three fundamental processes: ^{3}He(d,d)^{3}He; ^{3}He(d,p)^{4}He; and ^{4}He(p,p)^{4}He. The total number of _types_ of experiments, most as functions of excitation energy and and scattering angle, is 34. Some of them are differential cross sections, polarizations, polarization correlations, and polarization transfers, with the polarization experiments involving vector and tensor polarizations. Over the

energy range we have considered up to now, from low energy $^4He(p,p)^4He$ elastic scattering up to $^3He(d,d)^3He$ and $^3He(d,p)^4He$ processes with 10 MeV laboratory deuteron energies, there are now about 320 angular distributions at various energies in the data base with over 3500 data points.

For some time we have had a semi-quantitative description of this entire data base which reproduces almost all of the complicated angle and energy dependence of the various experiments. This result is tantalizing and not completely satisfactory for two reasons. The first is that one purpose of our analysis is to provide reliable quantitative predictions of the cross sections of practical interest. The other is that the theoretical approach we are using should, using the correct values of certain parameters that we are able to adjust, describe the experimental results with great accuracy.

A number of possible causes of the discrepancies come to mind.

1. The data is possibly inaccurate. In particular, the consistency of data in the different channels has been suspect.

2. The parameterization is not sufficiently flexible. The theory in principle requires an infinite number of parameters. The choice of a finite set is an approximation; and although we think we know how to do this in a good way, we may have not been clever enough.

3. The present solution is not correct. It is well known that single energy phase-shift analyses often have many spurious solutions in addition to the correct one. It is conceivable, although we have never seen an example, that an energy dependent analysis could find a false minimum by finding different spurious solutions at different energies.

4. The minimization process is not yet finished. This problem is so large that an inordinate amount of computer time would be required to reach final convergence of the data fitting process. It is only a selective judgment, based on other problems, when to abandon the minimization attempt and assume that further significant progress is unlikely.

Recently a number of considerations have refocussed rigorous attention on the ^5Li problem. There has been renewed interest in the $^3He(d,p)^4He$ reaction as a neutron-free thermonuclear energy source. In addition, a number of new experiments are finished or nearing completion. Finally, the EDA program has been brought up on CRAY, whose larger fast memory allows an increased scope to the problem, including possibly the inclusion of more adjustable parameters.

The new work has been designed to try to find the causes of our previous discrepancies and has proceeded along several lines. First, the new data,

primarily many experimental results from ETH at Zurich on the ^{3}He(d,d)^{3}He process and the new results from Ohio State on the ^{3}He(d,p)^{4}He process, have been included in the general analysis. Secondly, improved wisdom about the choice of parameters, gained from other problems, has been brought to bear. Finally, a number of subsidiary analyses using reduced data sets have been made. The results, still preliminary, are as follows.

Of the possible causes, only No. 3 is probably not involved, although No. 4 is probably not a major contributor. In particular, it is clear that the data are not entirely accurate or consistent, but it is also clear that inconsistency between channels is not the primary problem, if it is one at all. It is also clear that our parameterization is indeed insufficient. Since part of the problem is that we are up to the limit of the number of parameters permitted on the 7600, which amounts in any formulation of the problems we consider to be feasible to about 145, we are adopting a new strategy. A direct transfer to CRAY at this time is not considered since the EDA program is considerably more expensive on it than on the 7600. What we have now undertaken is the separation of the problem into two parts. In the first, only experiments at energies less than 5 MeV deuteron laboratory energy are considered. This allows a reduction in the number of parameters, and has already met with partial success over a limited data base. The energies over 5 MeV will be fitted with a parameterization not utilizing the resonance structure characterizing the usual R-matrix but still having many of its features. The plan is to combine these two problems on the CRAY for a final fine-tuning.

It is worth noting that in all of the work done so far there have been only slight differences in our results in the neighborhood of the resonance at approximately 450 keV, which is responsible for this interest in the ^{3}He(d,p)^{4}He reaction. We have never been able to predict a maximum value of the reaction greater than 0.83 b. This is below the value of 0.91 b commonly quoted.

C.   Calculations of Neutron Reactions on Isotopes of Nickel   [R. C. Harper (Graduate Research Assistant, Auburn U) and E. D. Arthur]

As part of a continuing effort to extend ENDF cross-section libraries up to the 50 MeV region, we have begun preliminary calculations of neutron reactions on the ^{58}Ni, ^{60}Ni, and ^{62}Ni isotopes. As with our earlier calculations[1,2] on ^{54}Fe, ^{56}Fe and ^{59}Co, a major effort has been made to determine and verify neutron, proton, and alpha-particle optical model parameters suitable for use over

a wide energy range. The resulting parameters appear in Table I. The neutron optical parameters were determined through simultaneous fits to reaction cross sections, elastic angular distributions, and total cross sections measured between 1 and 50 MeV. Through the additional constraint of experimental s- and p-wave strength data, these parameters are applicable over the energy range from a few hundred keV to 50 MeV. The proton optical parameters appearing in the table are a modified form of the Perey[3] parameter set that was verified and adjusted through comparison to low energy ^{59}Co(p,n) data, reaction cross sections from 9 to 60 MeV, and elastic scattering angular distributions between 18 and 39 MeV. The alpha particle optical parameters are the same as those employed in our iron and cobalt calculations. Comparisons of Hauser-Feshbach calculations to ^{54}Fe(α,n), (α,2n), and (α,p) data between 8 and 20 MeV indicated that no significant adjustments were needed to reasonably reproduce these experimental results. As a final step, discrete level information was assembled for nuclei between ^{51}Fe and ^{62}Ni. Gamma-ray strength functions were determined through fits to ^{58}Ni, ^{60}Ni, and ^{62}Ni (n, γ) data. DWBA calculations of direct inelastic scattering cross sections to collective states in ^{58}Ni, ^{60}Ni, and ^{62}Ni were made using the β_ℓ values deduced from proton inelastic scattering data.

With the GNASH[4] and COMNUC[5] nuclear-model codes, preliminary comparisons have been made to experimental data for natural nickel as well as for the separated ^{58}Ni, ^{60}Ni, and ^{62}Ni isotopes. Such data include inelastic scattering cross sections induced by 1.5- to 9-MeV neutrons; (n,p), (n,2n), (n,np), and (n, α) cross sections from threshold up to energies greater than 20 MeV; charged-particle production spectra produced by 15-MeV neutron interactions; and gamma-ray production spectra from 10 to 20 MeV. Good agreement was obtained in simultaneous comparisons to these data types. In particular, our calculation of the ^{58}Ni(n,2n) cross section agreed well with experimental data, particularly the recent results of Bayhurst et al.[6] (see Fig. 1). Such agreement is gratifying since the (n,2n) cross section accounts for only a small fraction of the total reaction cross section, a situation that produces strong constraints on both the neutron and charged-particle optical parameters. In fact, other published calculations[6,7] of this reaction overestimate it by factors of 2 to 4, leading to speculation about a breakdown of the statistical model in this case. Problems with these calculations seem to be with the parameters used rather than the model.

5

As a prelude to higher energy neutron cross-section calculations, GNASH results were compared to experimental data for [58]Ni(p,pn), (p,2p), (p,p2n), (p,2pn), and (p,α) reactions up to 40 MeV. The good agreement obtained provides further confirmation of the applicability of the optical parameters at higher energies as well as other facets of the calculation, particularly the level density and preequilibrium models used.

TABLE I

OPTICAL PARAMETERS

Neutrons	r(fm)	a(fm)
$V(\text{MeV}) = 50.06 - 0.372E$	1.278	0.56
$W_{vol}(\text{MeV}) = -0.941 + 0.197E$	1.287	0.56
$V_{SO}(\text{MeV}) = 6.2$	1.12	0.47
$W_{SD}(\text{MeV}) = 4.876 + 0.270E$	1.345	0.47
Above 6 MeV	1.345	0.47
$W_{SD}(\text{MeV}) = 6.497 - 0.225(E-6)$		

Protons	r(fm)	a(fm)
$V(\text{MeV}) = 53.3 + 27\left(\dfrac{N-Z}{A}\right) + \dfrac{0.4Z}{A^{1/3}} - 0.55E$	1.25	0.65
$V_{SO}(\text{MeV}) = 7.5$	1.25	0.47
$W_{SD}(\text{MeV}) = 13.5 - 0.1E$	1.25	0.47
$r_c(\text{fm}) = 1.25$		

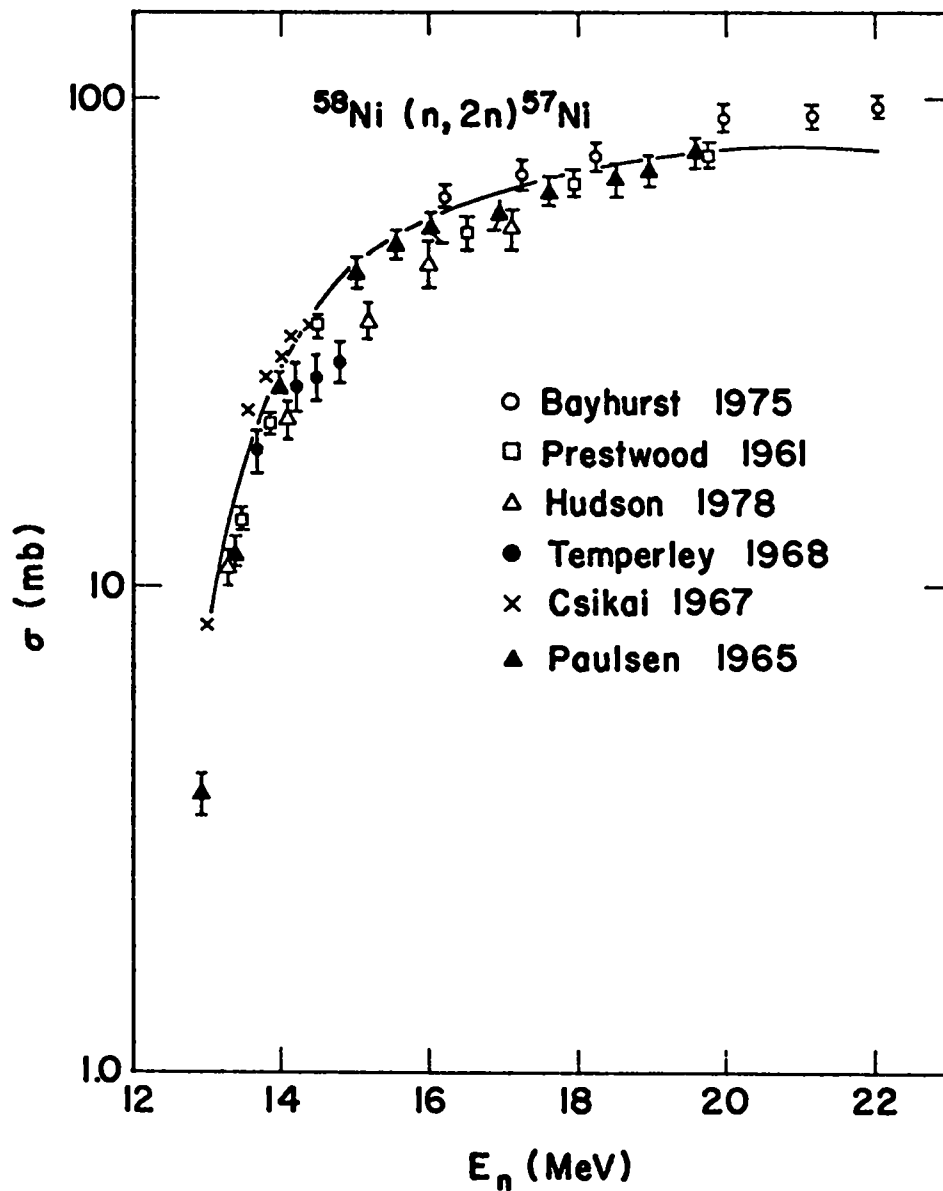| Alphas	r(fm)	a(fm)
$V(\text{MeV}) = 193 - 0.15E$	1.37	0.56
$W_{vol}(\text{MeV}) = 21 + 0.25E$	1.37	0.56
$r_c(\text{fm}) = 1.4$		

Fig. 1.
Calculated and experimental $^{58}Ni(n,2n)^{57}Ni$ cross-section values.

D. **Calculation of Prompt Fission Neutron Spectra and $\overline{\nu}_p$ [D. G. Madland and J. R. Nix (T-9)]**

An extensive journal article summarizing this work is in preparation. Our most recent communication presents calculations of the prompt fission neutron spectrum and $\overline{\nu}_p$ that include multiple-chance fission processes.[8]

Work is continuing on merging the codes for the energy-independent and energy-dependent compound-nucleus formation cross-section calculations. The merged code FISPEK is being modified to include internal checks and to print out warnings and error messages. Documentation for FISPEK has been started.

II. NUCLEAR CROSS SECTION PROCESSING

A. CSEWG Benchmarks and ENDF/B-V Processing (R. B. Kidman)

The 93-isotope, 70-group, ENDF/B-V library completed last quarter has been used to compute every Cross Section Evaluation Working Group (CSEWG) benchmark except SEFOR. The one-dimensional benchmark specifications were used to compute an extensive set of eigenvalues, central fluxes, central adjoints, edge spectra, central reaction rate ratios, central worths, central one-group cross sections, Rossi alphas, delayed neutron fractions, neutron lifetimes, and reactivity conversion factors. Some of the traditionally more popular results are shown in Table II. The complete set of results has been forwarded to CSEWG.

The relatively high computed eigenvalues of the small reflected assemblies BIGTEN, FLATTOP-25, FLATTOP-PU, FLATTOP-23, and THOR were investigated. The most probable cause is that the P_3 calculations are not sufficiently close to P_∞ i.e, P_5 cross sections are needed.

Other small and therefore bothersome effects can be attributed to not having elastic matrix f-factors and not having a fission source matrix. Therefore, we have decided to reprocess the multigrouping portion of the NJOY processing for at least the most important isotopes of the above library. The reprocessed isotopes will be in CCCC-IV format and will include P_5 cross sections, elastic removal f-factors, and fission source matrices.

B. NJOY Code Development (R. E. MacFarlane and R. M. Boicourt)

A new version of the NJOY nuclear data processing system is being prepared for release. The differences between the new NJOY (7/80) and the previous NJOY (1/80) for each module are as follows: for NJOY, change the version date, add a new routine for significant figure control, and add a repeat option to FREE; for

TABLE II

UNCORRECTED CSEWG BENCHMARKS RESULTS (C/E)

Benchmark	Eigenvalue	F28/F25	F49/F25	C28/F25
Pu Fueled[a]				
JEZEBEL (bare)	1.0094	0.9250	0.9717	
JEZEBEL-Pu (bare)	1.0008	0.9330		
THOR	1.0152	0.9247		0.8531
FLATTOP-Pu	1.0119	0.9307		
VERA-11A	0.9543	1.1733	1.1185	
ZEBRA-3	1.0037	1.0407	1.0094	
SNEAK-7A	0.9978	1.0250	1.0152	1.0032
SNEAK-7B	1.0054	1.0545	1.0255	1.0348
ZPR-3-48	0.9862	1.1243		0.9891
ZPR-3-56B	1.0059	1.0219	0.9776	
ZPR-9-31	0.9966	1.0934	1.0822	1.1119
ZPR-6-7	0.9835	1.0078	0.9934	1.0704
ZPPR-2	0.9835	1.1444		
U Fueled[a]				
JEZEBEL-23 (bare)	0.9947	1.0043		
FLATTOP-23	1.0055	0.9882		
GODIVA (bare)	1.0013	1.0350	0.9932	
FLATTOP-25	1.0092	1.0336	0.9995	
ZPR-3-6F	0.9969	1.0238	1.0360	0.9281
VERA-1B	0.9579	1.2707	1.1082	0.9050
ZPR-3-12	0.9968	1.1202	1.0305	0.9569
ZPR-3-11	1.0115	1.0789	1.0007	0.9674
BIGTEN	1.0157	1.0786	1.0066	0.9961
ZEBRA-2	0.9771	1.1271	1.0502	0.9968
ZPR-6-6A	0.9808	0.9865		1.0448

---

[a]The benchmarks are arranged from hardest to softest central spectra.

RECONR, implement the new method for significant figure control, add 0.0253 eV
to the energy grid, add a new capability to thin the resonance grid, and fix a
typographical error in the IBM conversion statements; for UNRESR, increase the
maximum number of dilution values to 8; for HEATR, provide a tolerance for a
test; for GROUPR, correct the final value of the computed flux, correct an error
in the choice of intermediate energies for tabulated weight functions, correct
the high-energy group of the discrete-level scattering matrices, make the user
weight function variably dimensioned, fix the unresolved fission cross section
for cases with second-chance fission, increase the number of subsections of
secondary-energy distribution data allowed, implement an option to selectively
add or replace reactions on an existing GROUPR output file, set undefined varia-
bles, and fix some statement numbers; for GAMINR, update GPANEL to be consistent
with PANEL in GROUPR; for ERROR, implement the new method to control significant
figures, add new group structure and weight function, add logic to allow files
without a total cross section to be processed (e.g., ENDF/B-V dosimetry files),
add option to selectively process reactions, and resequence some statement num-
bers; for DTFR, remove an unused common; for CCCCR, allow for isotopes with no
capture cross section, update BRKOXS file to the CCCC-IV standard including
self-shielding factor for elastic removal, modify the ISOTXS output file to al-
low for a fission chi matrix or for computing a chi vector with a user-specified
weight function, and correct a format statement; for MATXSR, correct the IBM
coding for BLOCK DATA and the logic to replace ENCODE, allow for different Le-
gendre orders in different data types, correct an error in handling all-zero
scattering matrices, correct a comment card, and correct one format; for ACER,
correct some of the IBM comment cards, fix the integral thinning option, imple-
ment the new logic for significant-figure control, allow for certain File 5 sec-
tions with two interpolation ranges, and set several uninitialized variables;
and for POWR, correct the conversion to atomic weight, add infinite dilution
shielding factor to tables, and set some unitialized variables.

C.   MAX Code Development (R. E. MacFarlane)

The new macroscopic cross-section code MAX is based on a diffusion-
accelerated discrete-ordinates transport code[9] being developed by LASL Group T-1
(Transport Theory). During this quarter, MAX was updated to be more consistent
with the latest T-1 code ONEDANT. It was observed that the eigenvalue produced

by the first outer iteration was not the correct diffusion eigenvalue. Subsequently, the ONEDA module in MAX was reorganized so that processing can be stopped after one outer iteration with results for eigenvalue, flux, and balance that are very close to those obtained with a conventional diffusion code such as 1DX.[10] This version also converges faster than previous versions for fast reactor problems.

Benchmark testing of ENDF/B-V cross sections with this version of MAX has revealed two problems with the 70-group fast reactor library. First, the fission chi vectors are slightly too "hot." This comes about because the library weighting function included a fusion peak. When the CCCC ISOTXS file was generated, the NJOY fission matrix was collapsed into a chi vector using this default spectrum. The CCCCR module has now been modified to output a chi matrix; henceforth, a user can form the best chi vector for his particular application. The second problem occurred for isotopes with second- and third-chance fission. The GROUPR module was retrieving an incorrect fission cross section for the calculation of the fission matrix. This, in turn, caused some small errors in $\bar{\nu}$. A new 70-group library is being produced.

D. Thermal Reactor Code Development (R. E. MacFarlane)

Recent comparisons of EPRI-CELL runs made at LASL, Oak Ridge National Laboratory (ORNL), and the Electric Power Research Institute (EPRI) have shown some differences between the various versions, and a cooperative effort is underway to explain and remove the problems.

One set of differences was traced to the interpolation of self-shielding factors. The standard EPRI-CELL used a polynomial interpolation routine that could produce severe oscillations for some kinds of input data. A new routine has been developed that divides the σ_0 range into three parts: for large σ_0, interpolation is done on $1/\sigma_0$; for intermediate values, on $\log(\sigma_0)$; and for values below the lower limit of the table, extrapolation is done as σ_0^2. This routine is less likely to diverge than the original coding.

The original LASL epithermal library for EPRI-CELL did not contain infinite-dilution shielding factors for the higher temperatures. Examination of the data has shown that these shielding factors are often appreciably different from 1.0; therefore, a new library has been produced that includes these values. It was necessary to redimension several arrays in EPRI-CELL and in the library maintenance code GAMTAP to support this new library.

11

More recent comparisons using the latest library have revealed several other minor code differences. These have been fixed, and the LASL and EPRI results are now in good agreement for a spectrum of test problems.

E. Consistent Self-Shielding of the Discrete-Ordinates Equation for Neutron Transport (R. E. MacFarlane)

Recent attempts to apply the new LASL macroscopic cross section code MAX to ENDF/B-V fast reactor benchmark calculations have shown that special care must be used when preparing self-shielded cross sections for use in discrete-ordinates transport codes. The correct choice of cross sections is implicit in the work of Bell, Hansen, and Sandmeier (BHS).[11] Following their argument, the multigroup Boltzmann equation in slab geometry is written

$$\mu \frac{\partial}{\partial z} \Psi_g(\mu,z) + \sum_{n=0}^{\infty} (2n+1) \, P_n(\mu) \, \sigma_{ntg}(z) \, \Psi_{ng}(z)$$

$$= S_g(\mu,z) + \sum_{n=0}^{\infty} (2n+1) \, P_n(\mu) \sum_{g'} \sigma_{ng \leftarrow g'}(z) \, \Psi_{ng'}(z) \quad , \tag{1}$$

where μ is the cosine of the discrete angle, z is the space coordinate, P_n are the Legendre polynomials, S_g is the external source and fission source, Ψ is the angular flux, and the flux moments are defined by

$$\Psi_{ng} = \frac{1}{2} \int_{-1}^{1} \Psi_g(\mu) \, P_n(\mu) \, d\mu \quad . \tag{2}$$

The cross sections for Eq. (1) are defined to preserve the reaction rate in each term as follows:

$$\sigma_{ntg} = \frac{\int_g \sigma_t(E) \, W_n(E) \, dE}{\int_g W_n(E) \, dE} \quad , \tag{3}$$

$$\sigma_{ng \leftarrow g'} = \frac{\int_g \int_{g'} \sigma_n(E \leftarrow E') W_n(E') \, dE' dE}{\int_{g'} W_n(E') \, dE'} \quad , \tag{4}$$

12

where $W_n(E)$ is a weighting function that should be close to the actual energy dependent flux moments to give good multigroup cross sections. When resonance self-shielding is important, the weight function is often approximated by

$$W_n(E) = \frac{C(E)}{[\sigma_0 + \sigma_t(E)]^{n+1}} \quad , \tag{5}$$

where C is a smooth function of E such as $1/E$ and σ_0 is a parameter that can be used to account for the effects of other isotopes or escape. In the resonance region, σ_{1tg} is typically smaller than σ_{0tg}.

Discrete-ordinates transport codes don't solve Eq. (1); instead, they solve

$$\mu \frac{\partial}{\partial z} \phi_g(\mu,z) + \sigma_g(Z) \phi_g(\mu,g) =$$

$$= S_g(\mu,z) + \sum_{n=0}^{N} (2n+1) P_n(\mu) \sum_{g'} \sigma_{g \leftarrow g'}^{(n)}(z) \phi_{ng'}(z) \quad . \tag{6}$$

The cross sections for Eq. (6) must be chosen to make ϕ as close to Ψ as possible, Matching terms gives

$$\sigma_{g \leftarrow g'}^{(n)} = \sigma_{ng \leftarrow g'} + \delta_{gg'} \lfloor \sigma_g - \sigma_{ntg} \rfloor \quad , \quad n \leq N \quad . \tag{7}$$

Note that the off-diagonal scattering terms are still defined properly by Eq. (4) but that there is some freedom in choosing discrete-ordinates "total" or "in-group" cross sections. BHS were concerned with choosing σ_g to mitigate the effect of truncating the Legendre expansion of the scattering source, and they evaluated several different recipes, thus giving rise to the "transport corrections" used in many neutronics calculations.

However, even when truncation effects can be neglected, Eq. (6) implies that a "transport correction" is required in the resonance range. Assume that $\sigma_{ng \leftarrow g'} = 0$ for $n > N$. For $N = 0$, it is natural to chose

$$\sigma_g = \sigma_{0tg} \quad , \tag{8}$$

and

$$\sigma^{(0)}_{g \leftarrow g'} = \sigma_{0g \leftarrow g'} \quad ; \tag{9}$$

but then

$$\sigma^{(n)}_{g \leftarrow g'} = \delta_{gg'} \lfloor \sigma_{0tg} - \sigma_{ntg} \rfloor \quad , \quad n > 0 \quad . \tag{10}$$

BHS call this the "consistent-P" approximation. Even though the basic scattering is isotropic, the discrete-ordinates cross sections are not! Since MAX assumes that $\sigma_{ntg} = \sigma_{1tg}$ for $n > 1$, the scattering matrix of Eq. (8) includes an additional δ-function of forward scattering. Obviously, the discrete-ordinates calculation should be made using

$$\sigma_g = \sigma_{1tg} \quad , \tag{11}$$

$$\sigma^{(0)}_{g \leftarrow g'} = \sigma_{0g \leftarrow g'} - \delta_{gg'} \lfloor \sigma_{0tg} - \sigma_{1tg} \rfloor \quad , \tag{12}$$

$$\sigma^{(n)}_{g \leftarrow g'} = 0 \quad , \quad n > 0 \quad . \tag{13}$$

This probably should be called the "inconsistent-P" option since different expansion orders are used for the total cross section and the scattering matrix. In general,

$$\sigma_g = \sigma_{N+1,tg} \quad , \tag{14}$$

$$\sigma^{(n)}_{g \leftarrow g'} = \sigma_{ng \leftarrow g'} + \delta_{gg'} \lfloor \sigma_{N+1,tg} - \sigma_{ntg} \rfloor \quad . \tag{15}$$

This inconsistent-P approximation becomes equivalent to the BHS "extended transport correction" when scattering terms above order N are very small.

To demonstrate that these considerations have some practical importance, the CSEWG benchmark[12] based on ZPR-6 assembly 7 critical experiment was analyzed with no transport correction and with the BHS "extended" transport correction with the results shown in Table III.

14

TABLE III

RESULTS OF USING CONSISTENTLY SELF-SHIELDED TRANSPORT CROSS SECTIONS FOR THE ZPR-6/7 CRITICAL ASSEMBLY

Integral Parameter	Without Correction[a]	With Correction[a]
k_{eff}	1.0067	1.0026
U238 fis/Pu239 fis	0.9949	0.9997
U238 capt/Pu239 fis	1.067	1.065
U238 fis/Pu239 fis	1.013	1.012

---

[a]Results are calculated/experimental with heterogeniety corrections applied.

III. FISSION PRODUCT AND ACTINIDES: YIELDS, DECAY DATA, DEPLETION, AND BUILDUP

A. Application of Aggregate Fission-Product Impulse Fits [R. J. LaBauve, D. C. George, T. R. England, and C.W. Maynard (U. of Wisconsin)]

C. V. Chester of Oak Ridge National Laboratory asked us to calculate gamma and beta energy of spent fuel for a typical reactor condition (10 000 hours irradiation time and a few cooling times ranging from 1 week to 1 year), using the analytic pulse functions we previously developed.[13] In response to this request, we calculated gamma and beta spectra for the aggregate of fission products released from fissioning of both ^{235}U and ^{239}Pu.

In these calculations, we assumed a constant flux of 1×10^{13} n/cm^2-s induced by thermal reactions, and we obtained the spectra in units of MeV/fis and particles/fis. Six cooling times were chosen, namely, one week, two weeks, one month, two months, six months, and one year. Samples of our results are shown in Figs. 2-7. The requestor's prime interest was for the beta spectra, hence the inclusion of these illustrative plots. However, both beta and gamma spectra were requested.

We have also used the FITPULS code[14] to generate aggregate fission-product impluse fits that will be used illustrating a journal article being prepared for Nuclear Technology. These are in 6 energy groups with bounds at 0, 1, 2, 3, 4, 5, and 7.5 MeV and include fits for beta and gamma spectra for the aggregate of
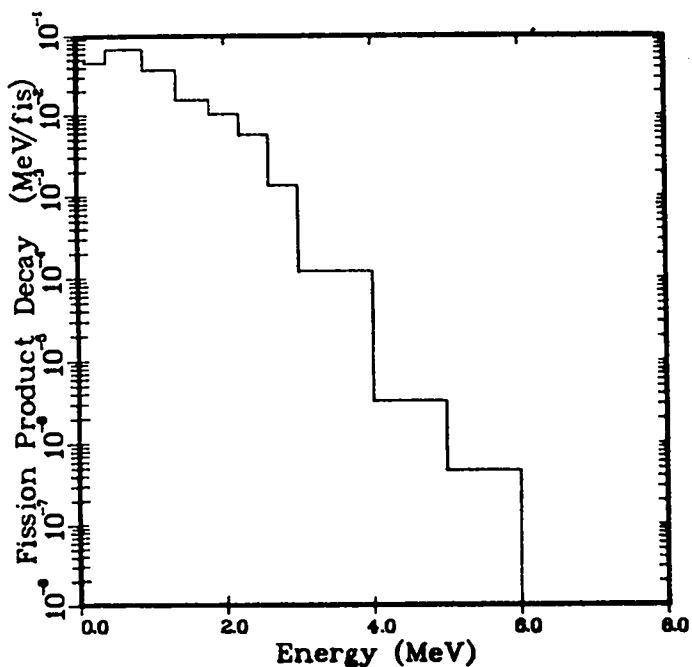
Fig. 2.
Beta spectrum for cooling
time 6 x 10^5 s.
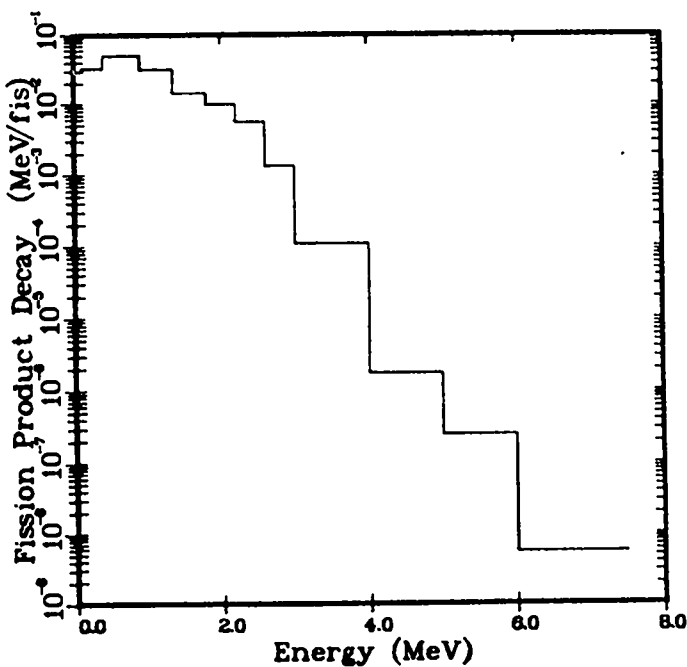
Fig. 3.
Beta spectrum for cooling
time 1.2 x 10^6 s.
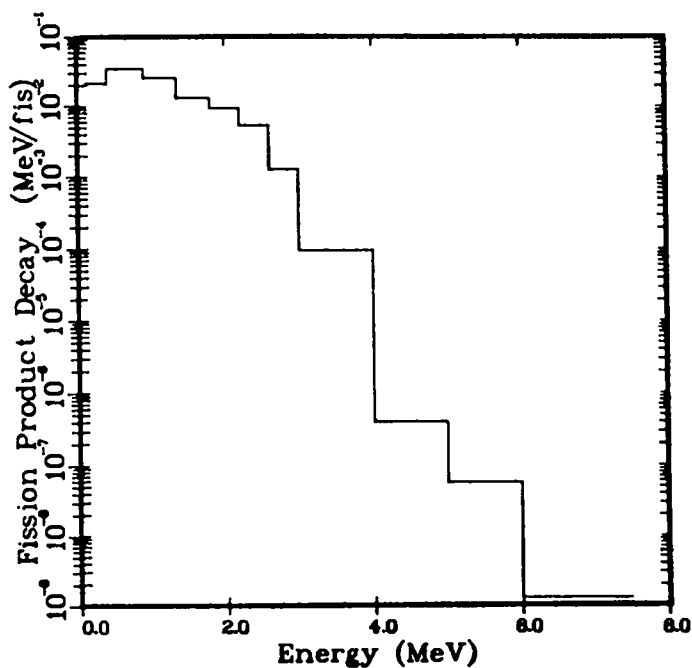
Fig. 4.
Beta spectrum for cooling
time 2.6 x 10^6 s.
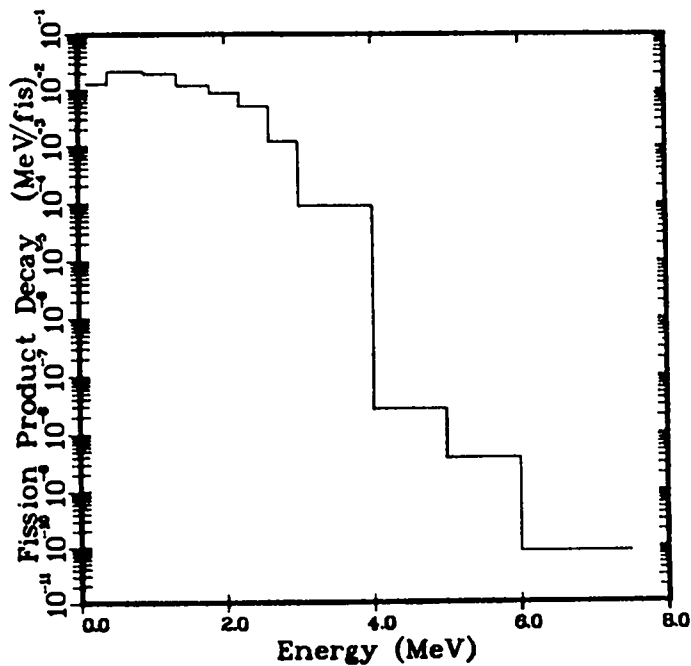
Fig. 5.
Beta spectrum for cooling
time 5.3 x 10^6 s.

16
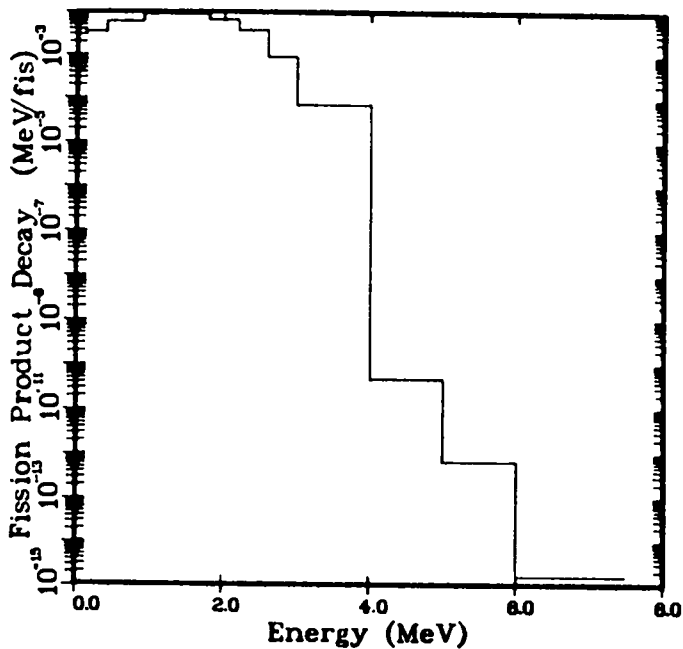
Fig. 6.
Beta spectrum for cooling
time 1.6 x 10^{7} s.
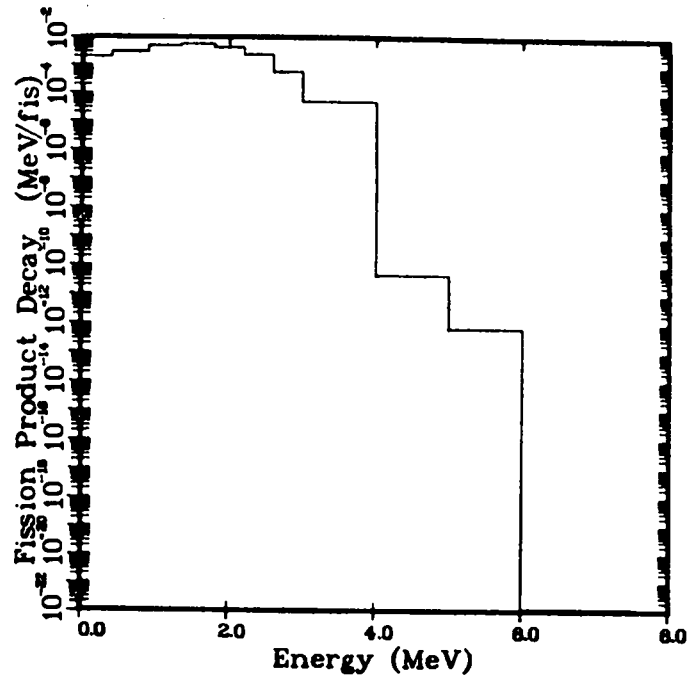
Fig. 7.
Beta spectrum for cooling
time 3.2 x 10^{7} s.

all fission products and the aggregate of all gaseous fission products resulting
from fission induced by thermal neutrons incident on both ^{235}U and ^{239}Pu.

B. Average Fission Product Cross Sections for BAPL (W. B. Wilson, T. R.
England, and N. L. Whittemore

The Bettis Atomic Power Laboratory (BAPL) uses the EPRI-CINDER code and its
library of processed ENDF/B-IV data. We supplied, at their request, 5-group
cross sections for 181 nuclides. These were collapsed using the TOAFEW code,
weighted with the PRS flux spectra.[15] BAPL intends to further group the cross
sections into three and four groups, depending on the specific design project.
For this purpose they chose the following five group energy bounds.

Few Group	Energy Bound	PRS Multigroups
	10 MeV	
1		7-17
	820.84 keV	
2		18-46
	5530.8 eV	
3		47-86
	10.677 eV	
4		87-127
	0.625 eV	
5		128-154
	10^{-5} eV	

C. ENDF/B-V Yields for CINDER Codes (T. R. England, W. B. Wilson, and N. L. Whittemore)

The various CINDER codes and all other summation codes using ENDF/B-V data must adjust the fission yields to account for nuclides that are not common to the decay and yield files. Table IV lists those nuclides not in the yield files and also those not in the decay files; all are in isomeric states. In several cases the adjustment is not significant, but in many cases it is essential to a correct total yield.

We have completed the adjustment for independent yields and for the CINDER-10 yield deck.

D. Actinide Decay Data (M. E. Battat, W. B. Wilson, R. J. LaBauve, and T. R. England)

ENDF/B-V contains decay data for 60 actinides; the major parameters for these were listed in the last progress report. During a reactor lifetime and subsequent decay of unprocessed spent fuel waste, there are 144 heavy mass nuclides that will be formed. Calculation of actinide content, particularly of the long-term waste content, requires an augmentation of the ENDF/B-V data.

The EBARDK code, described in the last progress report, has been used to generate beta-, gamma-, and alpha-decay energies for all 144 nuclides. In several cases the gamma spectrum has also been generated by the code. Data from the 60 nuclides common to ENDF/B-V will be used as an independent test of ENDF/B-V data; however, ENDF/B-V will be used in place of the EBARDK code results unless a significant error is indicated.

TABLE IV

NUCLIDES NOT COMMON TO ENDF/B-V YIELD AND DECAY FILES

Nuclides Not in Yield Files			Nuclides Not in Decay Files		
Z	A	State	Z	A	State
31	72	1	33	74	1
31	74	1	34	73	1
32	79	1	34	85	1
33	84	1	35	77	1
36	79	1	36	86	1
37	86	1	43	95	1
38	85	1	45	101	1
39	90	1	45	102	1
39	91	1	47	105	1
39	93	1	47	106	1
40	90	1	49	112	1
41	102	1	51	118	1
41	104	1	51	120	1
42	93	1	58	139	1
44	109	1	62	142	1
47	108	1	65	136	1
47	109	1	65	158	1
47	120	1	65	162	1
48	121	1	67	159	1
49	116	2	67	161	1
49	118	2	67	162	1
49	124	1	67	163	1
49	128	1	67	164	1
50	113	1	67	170	1
50	117	1			
51	124	2			
51	126	2			
52	121	1			
53	132	1			
54	125	1			
54	127	1			
54	129	1			
54	143	1			
55	135	1			
55	136	1			
56	135	1			
56	136	1			
59	142	1			
61	152	2			
63	152	2			

Data storage for the nuclides include beta endpoint energies, alpha energies, branching fractions, Q-values, spins, and parities. As noted, gamma energies and intensities are also included for some of the nuclides.

A module to compute the beta-decay spectra has been completed but not yet added to the code. To date, the total gamma-transition energy is calculated along with the average beta and alpha energy and alpha spectra, but the electron conversion is not separated from the gamma-transition value. The calculated transition energy has been compared to values from the GAMDAT-78[16] file and the difference matches the electron conversion energy in those cases where the conversion value is known. Therefore, we intend to complete the preliminary file of recoverable energies and spectra using (1) ENDF/B-V for 60 nuclides; (2) GAMDAT-78[16] for x-ray and gamma spectra in most cases; (3) beta and gamma spectra computed by the EBARDK code in other cases; and (4) beta spectra normalized to the sum of the EBARDK code value and the difference between the gamma-transition energy computed by EBARDK and the GAMDAT-78 value.

A few of the nuclides will require additional evaluation (e.g., where the gamma-transition energy is significantly smaller than the GAMDAT-78 value).

E.   The (α,n) Neutron Production by Alpha Particles in PuO_2, UO_2, and ThO_2 Fuels [R. T. Perry (U. of Wisconsin) and W. B. Wilson]

As a part of the evaluation of the long-term decay properties of spent reactor fuels, we calculated the (α,n) neutron production functions $P(E_\alpha)$ for several reactor fuels of interest. Neutron production functions have been calculated in the past;[17][18] however, they have not been developed specifically for the fuels of our interest. In particular, the change in $P(E_\alpha)$ due to burnup has not been considered.

In oxide fuels the primary source of (α,n) neutrons are from the alpha reactions with ^{17}O and ^{18}O. The neutron yield $P(E_\alpha)$ may be determined using the following relationship,

$$P(E_\alpha) = \int_0^{E_\alpha} \frac{\Sigma(E)}{\varepsilon(E)} \, dE \quad , \tag{16}$$

where $\Sigma(E)$ is the macroscopic oxygen (α,n) cross section and $\varepsilon(E)$ is the stopping power of the fuel, taken as the sum of the individual stopping powers of the elements in the fuel, each weighted according to the Bragg Rule.[19]

In establishing the methodology and data used for the calculations, we essentially followed the work of Ombrellaro and Johnson.[17] From 0 to approximately 5 MeV we used the Bair et al.[20,21] ^{17}O and ^{18}O (α,n) cross sections, which we multiplied by 1.35 for renormalization, as suggested by Bair.[22] From approximately 5 to 10 MeV we used the Hansen et al.[23] ^{17}O and ^{18}O (α,n) cross sections, which we multiplied by 0.908, again for renormalization. This factor was obtained by dividing the integral of the Bair and del Campo[22] natural oxygen cross sections by the sum of the integrals of the Hansen cross sections for ^{17}O and ^{18}O times their respective atom fractions in natural oxygen. The integrals were evaluated from 5.15 to 8 MeV. The Bair natural oxygen cross sections represent a more recent evaluation; however, we wished to look at the individual ^{17}O and ^{18}O contributions. Thus, we chose this renormalization, which had been used in previous work.[17]

With the exception of plutonium, for which no tabulated data exist in the literature, we used the stopping powers calculated by Ziegler.[24] To obtain stopping powers for plutonium, we used the theoretical ratios of stopping powers calculated by Northcliffe and Schilling[25] to calculate the ratios of the stopping powers of plutonium to uranium. We used these ratios with Ziegler's data for uranium to obtain values for plutonium. Using the methods of least squares, we fit our plutonium data to a polynomial and obtained

$$\ln(\varepsilon_{pu}) = 5.1486 - 0.171158(Z) - 0.272723(Z)^2$$

$$+ \ 0.100975(Z)^3 - 0.0160365(Z)^3 \quad , \tag{17}$$

where $Z = \ln(E)$. The stopping power ε_{pu} for plutonium has units of $eV/10^{15}$ atoms/cm^2 and E, the alpha particles energy, has units of MeV.

Table V is a list of the compositions of the reactor fuels we considered. They represent thermal reactor fuel, spent thermal reactor fuel, a U/Th system fuel, and a fast reactor fuel. For the spent thermal reactor fuel, we used niobium and praseodymium to represent the fission products, and number densities for neptunium, americium, and curium were added to those for plutonium in our calculations for this case.

The results of our calculations for the case representing spent thermal reactor fuel is plotted in Fig. 8, which shows $P(E_\alpha)$ as a function of the alpha particles' initial energy. The results for the remaining cases fall within 4% of these values. These results were obtained by the numerical integral of Eq. (16).

As a result of this work we have obtained an estimate of the stopping power for plutonium. We have calculated the neutron yields for four specific fission reactor fuels. We found that the neutron yields for these oxide fuels lie within 4% of each other and that burnup had little effect on the results. The combination of actinide alpha-particle energies and intensities described in Sec. III D with the LWR neutron production function $P(E_\alpha)$ yields effective $\bar{\nu}(\alpha,n)$ values for alpha emitters. This work is in progress for the approximately 90 actinide nuclides decaying at least partly by alpha emission.

TABLE V

FUEL COMPOSITIONS

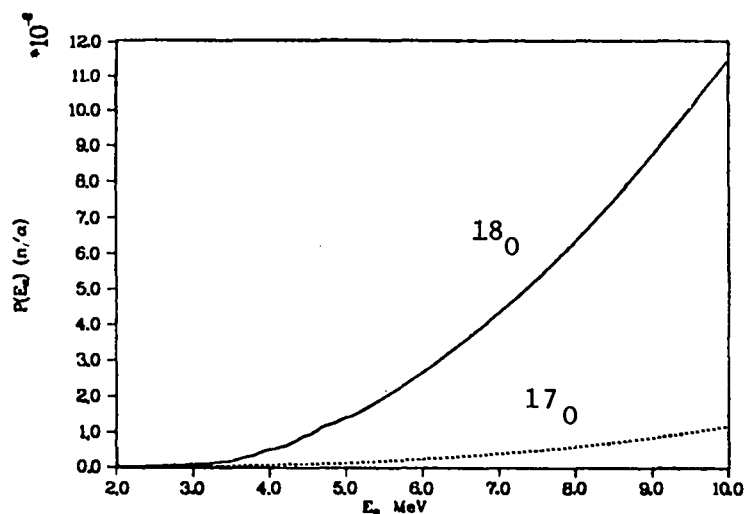| Fuel Elements (Densities given in at./b-cm)	Reactor Fuels			
	Thermal 9.95 gm/cm^3 (Beginning of life)	Thermal 9.95 gm/cm^3 34 GWd/t (15 months cooling)	U/TH 9.17 gm/cm^3 (Beginning of life)	Fast 9.62 gm/cm^3 (Beginning of life)
$_8$O	0.04372	0.04372	0.04184	0.04215
$_{41}$Nb		7.893x10^{-4}		
$_{59}$Pr		7.893x10^{-4}		
$_{90}$Th			0.02025	
$_{92}$U	0.02186	0.02085	6.72x10^{-4}	0.01887
$_{93}$Np		1.043x10^{-5}		
$_{94}$Pu		2.037x10^{-4}		0.002634
$_{95}$Am		5.692x10^{-6}		
$_{96}$Cm		1.131x10^{-6}		

Fig. 8.

Neutron production probability for decay alphas in LWR irradiated UO_2 fuel.

F. CINDER-10 ENDF/B-V Chain Structure [D. E. Wessol (EG&G, Idaho), T. R. England, and N. L. Whittemore]

ENDF/B-V now includes 877 fission products and revised decay branching fractions. A summary of the data types was included in the last progress report. The added nuclides and branching (e.g., there are 105 delayed neutron branchings now compared to 57 in ENDF/B-IV) require a revision in the CINDER-10 chain structure. This revision was completed during this quarter and required more than 100 additional linear chains and changes in existing chains. These are now being checked for errors. New cross-section and decay-data libraries are not yet complete.

G. ENDF/B-V Fission Product Consistency Check (T. R. England and N. L. Whittemore)

A review of the ENDF/B-V decay files has continued during this quarter using the spectral code described in the last progress report. Table VI lists all nuclides showing a discrepancy in average beta, total gamma, and total recoverable energy, or in Q-values as listed in the preliminary files and as calculated from the decay spectra. Only values differing by more than 5% in Q and less than 3% in the other energies are listed. This is simply a consistency test and is possible only for the 265 nuclides having spectra. A total of 750 nuclides are unstable; all require some review of their preliminary data. Such a review is in progress at the Los Alamos Scientific Laboratory, Hanford Engineering Development Laboratory, Idaho Nuclear Engineering Laboratory, and in England (A. Tobias).

TABLE VI

ENDF/B-V CONSISTENCY OF COMPUTED ENERGIES FROM SPECTRA WITH AVERAGE IN FILE

Nuclide	% Deviation			
	E_β	E_γ	E_{tot}	Q
*35-Br-82m	1	1.8	1	56.8
35-Br-87	0	0	0	- 5.4
35-Br-88	0	1	1	- 6.2
36-Kr-83m	4.6	1	4.3	5.7
*36-Kr-85	10.3	0	10.2	0
37-Rb-90	0	0	0	6.0
*38-Sr-90	12.9	--	12.9	0
39-Y-91m	6.0	0	1	1
39-Y-95	1	1	1	- 5.9
*40-Zr-93	22.0	.--	22.4	49.0
41-Nb-93m	5.6	1	5.3	7.5
*41-Nb-94	15.7	0	1.2	2.5
41-Nb-97m	5.0	0	1	1
43-Tc-99m	3.7	0	1	1
43-Tc-102	- 3.0	0	- 2.4	0
45-Rh-103m	4.4	1	4.2	5.7
45-Rh-104	1	-3.5	1	1
45-Rh-104m	4.4	0	2.62	2.64
46-Pd-107	9.5	--	9.5	0
46-Pd-112	1	0	1	6.45
47-Ag-108m	6.7	0	0	1
47-Ag-109m	3.2	0	2.77	3.80
47-Ag-111m	4.6	1	4.11	5.27
*48-Cd-109	0	0	0	17.26
48-Cd-113m	1	1	1	- 5.11
*49-In-118m	0	0	0	-69.79
*50-In-119m	1	1	1	-58.48
*50-In-121m	14.2	1	12.0	1
*51-Sb-126	6.10	1	6.02	100.4
*51-Sb-131	1	0	0	-10.09
52-Te-131m	1	1	0	5.42
*52-Te-133m	1	0	0	-27.08
*53-I-134m	- 1.03	0	0	47.4
54-Xe-139	1	1	1	5.75
55-Cs-137	9.30	--	9.30	1
55-Cs-141	1	-3.-6	- 1.51	- 5.23
56-Ba-140	1.30	0	1	- 6.89
57-La-142	1	-1.10	1	- 9.98
59-Pr-148	-1.09	0	1	- 6.57
*61-Fm-151m	1	1	1	-15.27
*63-Eu-152m	7.58	0	3.23	12.27

*These 15 nuclides show significant inconsistencies as underlined.

H. Compact Representation of Neutron Activation and Decay Data in Decay-Dominated Applications (D. W. Muir)

In a number of neutron activation applications involving either relatively low neutron-flux levels or hardened neutron spectra, it is a good approximation to neglect the effect of neutron reactions, in comparison with radioactive decay, when calculating the rates of depletion and transmutation of all radioactive species present. We have developed a new method for constructing a calculation-oriented nuclear-data library to describe, as compactly as possible, activation and decay processes in such "decay-dominated" applications.

By transforming the input data library in the way described below, one avoids the need to solve during the actual decay calculations the fully coupled differential equations usually used to describe sequential radioactive decay with branching. Instead, one needs only to solve the simpler equations for independent (single-step) decay. With this approach, one also avoids the need to store the matrix of decay branching ratios, which can be the largest part of the input data library.

One promising area of application of this approach is in calculations of decay gamma-ray dose rates, especially when relatively low neutron fluxes are involved. Particular applications might include near-term fusion device design,[26] neutron radiotherapy studies,[27] and high-energy-accelerator target design.[28]

The method may also be useful at reactor-like flux levels (up to perhaps 10^{15} n/cm^2 s), provided the neutron flux below a few keV is suppressed, for example, by the presence of neutron absorbers such as lithium or boron. (This restriction is necessary because of the great variability of low-energy neutron reaction cross sections.) In such a hardened neutron spectrum, the spectrum-averaged (n,γ) cross section for any radioactive isotope that can be produced by irradiation of the common structural materials will be less than 1 b.[29,30] With a neutron flux of 10^{15} n/cm^2 s, this cross section converts to an effective half-life of 22 years. For many applications, this can be considered a negligibly slow process in comparison with radioactive decay.

We consider a target material (which may be an isotope, an element, or a mixture of elements) that under neutron irradiation yields J distinct radioactive species X_j. The species X_j can be produced directly by neutron reactions and/or indirectly by a neutron reaction followed by radioactive decay. In some cases of interest (for example, 14-MeV neutron irradiation of molybdenum,

stainless steel, or concrete), as many as 30 distinct radioactive species can be produced directly or indirectly from a single target material.

Let $n_j(t)$ be the number of atoms of X_j that are present at time t, following the irradiation of the specified target material by a short pulse of neutrons at t = 0, per atom of the target material. In the absence of neutron reactions with the radioactive products, one can construct the solution for a general time-dependent neutron source by superimposing solutions for such a pulsed-source case.

Let $\underline{N}$ be a column matrix formed from the J elements $n_j(t)$. The initial conditions $\underline{N}(0)$ can be obtained from the following matrix equation,

$$\underline{N}(0) = \underline{\Sigma} \; \underline{\Phi}(0) \quad . \tag{18}$$

Here $\underline{\Phi}(0)$ is a column matix with K elements $\phi_k(0)$, which specify the zero-time fluence in the k-th neutron energy group. $\underline{\Sigma}$ is a rectangular matrix with J rows and K columns. The elements σ_{jk} of $\underline{\Sigma}$ are the microscopic cross sections for the production of species X_j by neutrons in energy group k.

Following the pulsed irradiation, the time evolution of $\underline{N}$ is governed by the well-known matrix equation

$$\frac{d}{dt} \underline{N} = \underline{D} \; \underline{N} \quad . \tag{19}$$

The diagonal elements of the J x J decay matrix $\underline{D}$ are the usual decay constants, $d_{ii} = -\lambda_i$. The off-diagonal elements d_{ij} are equal to $\lambda_j \, p_{ji}$, where p_{ji} is the branching ratio for the decay of X_j into X_i. Because of energy conservation, the species can always be indexed so that $d_{ij} = 0$ for j > i. We assume $\underline{D}$ has this triangular form.

In the applications of interest, the induced radioactivity is not localized but distributed over a large region, over which the neutron energy spectrum $\underline{\Phi}(0)$ may vary significantly. In such cases, the initial conditions $\underline{N}(0)$ become space dependent, so the decay equations must be solved at every space point in the system.

Although one cannot entirely avoid the need to solve Eqs. (18) and (19) at each space point, one can reformulate these equations so that their solution is greatly simplified. This reformulation begins with the introduction of a new

set of J time-dependent functions $\underline{N}^*$, related to the original $\underline{N}$ by a J x J matrix of constant coefficients $\underline{A}$,

$$\underline{N}^* = \underline{A}\ \underline{N} \quad . \tag{20}$$

As shown below, $\underline{A}$ can be chosen so that the new functions $\underline{N}^*$ satisfy the far simpler decay equations

$$\frac{d}{dt}\ \underline{N}^* = \underline{D}^*\ \underline{N}^* \quad , \tag{21}$$

where $\underline{D}^*$ contains the same diagonal elements as $\underline{D}$, $d^*_{ii} = -\lambda_i$, but the off-diagonal elements of $\underline{D}^*$ are all zero. The solutions $n^*_i(t)$ of Eq. (21) are simply $n^*_i(0)\ e^{-\lambda_i t}$.

Eliminating $\underline{N}^*$ from Eq. (21) using Eq. (20) and then substituting from Eq. (19), one obtains the following condition on the transformation matrix $\underline{A}$:

$$\underline{A}\ \underline{D} = \underline{D}^*\ \underline{A} \quad . \tag{22}$$

One can show that the following prescription for the elements of $\underline{A}$ satisfies Eq. (22), which guarantees that $\underline{N}^*$ satisfies Eq. (21). For i ranging from 1 to J,

$$a_{ij} = \begin{cases} 0, & \text{if } j > i; \\ 1, & \text{if } j = i; \\ \displaystyle\sum_{k=j+1}^{i} \frac{a_{ik}\,d_{kj}}{\lambda_j - \lambda_i} & , \text{if } j < i \quad . \end{cases} \tag{23}$$

Equation (23) can be applied repeatedly to calculate each a_{ij}, proceeding from high to low j-values for a given value of i.

It is important to note that, while the matrix $\underline{A}$ depends on the target material in question (through $\underline{D}$), it is problem-independent. That is, $\underline{A}$ does not depend on the particular irradiation conditions.

The initial conditions for the decoupled decay equations, Eq. (21), can be obtained directly from the zero-time neutron fluence by employing a set of transformed activation cross sections. If the cross sections are transformed according to

$$\underline{\Sigma}^* = \underline{A} \ \underline{\Sigma} \quad , \tag{24}$$

then from Eqs. (18), (20), and (24)

$$\underline{N}^*(0) = \underline{\Sigma}^* \ \underline{\Phi}(0) \quad . \tag{25}$$

Turning to the decay data, we first note that the matrix $\underline{A}$, Eq. (23), has a non-zero determinant so that $\underline{A}^{-1}$ exists. This is important because it means that one can calculate any desired radionuclide effect, such as delayed local heating (afterheat), total biological hazard potention (BHP), or decay gamma-ray source strength, directly from $\underline{N}^*$ without ever having to calculate the original, coupled concentrations $\underline{N}$.

This can be shown most easily by considering a particular example, such as the emission of decay gamma rays. Let $\underline{Q}$ be a column matrix with M elements $q_m(t)$ equal to the rate of emission of gamma rays in (gamma-ray) energy group m, per atom of the target nuclide. Then,

$$\underline{Q} = \underline{S} \ \underline{N} \quad , \tag{26}$$

where $\underline{S}$ is a rectangular matrix with M rows and J columns. The elements s_{mj} of of $\underline{S}$ give the emission rate in gamma-ray energy group m, per atom of radioactive species X_j present. Since $\underline{A}^{-1}$ exists, Eq. (20) can be rewritten as

$$\underline{N} = \underline{A}^{-1} \ \underline{N}^* \quad . \tag{27}$$

Combining Eqs. (26) and (27),

$$\underline{Q} = \underline{S} \ (\underline{A}^{-1} \ \underline{N}^*) = (\underline{S} \ \underline{A}^{-1}) \ N^* \quad . \tag{28}$$

Since $\underline{S}$ and $\underline{A}^{-1}$ are both problem-independent, we can combine them to generate a new problem-independent matrix

$$\underline{S}^* = \underline{S} \ \underline{A}^{-1} \quad . \tag{29}$$

From Eq. (28) it can be seen that the new matrix $\underline{S}^*$ can be used along with the problem-dependent (but simply calculated) $\underline{N}^*$ to calculate a correct, delayed gamma-ray source,

$$\underline{Q} = \underline{S}^* \; \underline{N}^* \quad . \tag{30}$$

Because $\underline{A}$ is triangular [see Eq. (23)], the elements of $\underline{S}^*$ can be obtained directly in terms of the a_{ij} without explicitly calculating $\underline{A}^{-1}$. Multiplying Eq. (29) from the right with $\underline{A}$ and recalling that $a_{ii} = 1$, one obtains the following prescription. For m ranging from 1 to M,

$$s^*_{mj} = \begin{cases} s_{mj}, & \text{if } j = J; \\ s_{mj} - \displaystyle\sum_{k=j+1}^{J} s^*_{mk} \, a_{kj}, & \text{if } j < J. \end{cases} \tag{31}$$

From this last result it is clear that, except for the case $j = J$, the individual s^*_{mj} are not simply related to the gamma-ray emission rates of any one nuclide. In fact, some of them may even be negative. (This is also true of the transformed cross sections.) Thus, the calculational efficiency gained by transforming the activation and decay data in this way is accompanied by some loss of data interpretability.

REFERENCES

1. E. D. Arthur and P. G. Young, "Evaluation of Neutron Cross Sections to 40 MeV for $^{54, 56}$Fe," presented at the Symp. on Neutron Cross Sections from 10 to 50 MeV, Brookhaven National Laboratory (May 1980).

2. E. D. Arthur, P. G. Young, and W. K. Mathes, "Calculations of ^{59}Co Neutron Cross Sections between 3 and 50 MeV," presented at the Symp. on Neutron Cross Sections from 10 to 50 MeV, Brookhaven National Laboratory (May 1980).

3. F. G. Perey, "Optical Model Analysis of Proton Elastic Scattering in the Range of 9 to 22 MeV," Phys. Rev. 131, 745 (1962).

4. P. G. Young and E. D. Arthur, "GNASH: A Preequilibrium Statistical Nuclear-Model Code for Calculation of Cross Sections and Emission Spectra," Los Alamos Scientific Laboratory report LA-6947 (Nov. 1977).

5. C. L. Dunford, "A Unified Model for Analysis of Compound Nucleus Reactions," Atomic International report AI-AEC-12931 (July 1970).

6. B. P. Bayhurst, J. S. Gilmore, R. J. Prestwood, J. B. Wilhelmy, Nelson Jarmie, B. H. Erkkila, and R. A. Hardekopf, "Cross Sections for (n,xn) Reactions between 7.5 and 28 MeV," Phys. Rev. C12, 451 (1975).

7. A. Marcinkowski, "Measurements and Evaluation of Fast Neutron Cross Section Data for Reactor Dosimetry," Proc. Advisory Group Meeting on Nuclear Data for Reactor Dosimetry, International Atomic Energy Agency report INDC(NDS)=103/M (1979).

8. David G. Madland and J. Rayford Nix, "Calculation of Neutron Spectra and Average Neutron Multiplicities from Fission," submitted for presentation at the Int. Conf. on Nuclear Physics, Berkeley, CA (Aug. 24-30, 1980).

9. R. E. Alcouffe, "Diffusion Synthetic Acceleration Methods for the Diamond-Differenced Discrete-Ordinates Equations," Nucl. Sci. Eng. 64, 344 (1977).

10. R. W. Hardie and W. W. Little, Jr., "1DX, A One-Dimentsional Diffusion Code for Generating Effective Nuclear Cross Sections," Battelle Northwest Laboratory report BNWL-954 (1969).

11. G. I. Bell, G. E. Hansen, and H. A. Sandmeier, "Multitable Treatments of Anisotropic Sattering in S_n Multigroup Transport Calculations," Nucl. Sci. Eng. 28, 376 (1967).

12. "Cross Section Evaluation Working Group Benchmark Specifications," Brookhaven National Laboratory report BNL-19302 (ENDF-202) (Nov. 1974).

13. R. J. LaBauve, T. R. England, D. C. George, and M. G. Stamatelatos, "The Application of a Library of Processed ENDF/B-IV Fission Product Aggregate Decay Data in the Calculation of Decay-Energy Spectra," Los Alamos Scientific Laboratory report LA-7483-MS (Sept. 1978).

14. R. J. LaBauve, D. C. George, and T. R. England, "FITPULS, A Code for Obtaining Analytic Fits to Aggregate Fission-Product Decay Energy Spectra," Los Alamos Scientific Laboratory report LA-8277-MS (March 1980).

15. W. B. Wilson and T. R. England, "Multigroup and Few-Group Cross Sections for ENDF/B-IV Fission Products, the TOAFEW Collapsing Code and Data File of 154-Group Fission-Product Cross Sections, Los Alamos Scientific Laboratory report LA-7174-MS (March 1978).

16. Gerhard Erdtmann and Werner Soyka, The Gamma Rays of the Radionuclides: Tables for Applied Gamma Ray Spectrometry (Weinheim, New York; Verlag Chemie, 1979).

17. P. A. Ombrellaro and D. L. Johnson, "Subcritical Reactivity Monitoring: Neutron Yields from Spontaneous (α,n) Reactions in FFTF Fuel," Hanford Engineering Development Laboratory report HEDL-TME 78-39 (June 1978). (Information contained in this report has been updated and supplemented by personal communication with the authors.)

18. H. Liskien and A. Paulsen, "Neutron Yields of Light Elements under α-Bombardment," Atomkernenergie $\underline{30}$, 59 (1977).

19. W. H. Bragg and R. Kleeman, "On the α Particles of Radium, and Their Loss of Range in Passing Through Varius Atoms and Molecules," Philos. Mag. $\underline{10}$, 318 (1905).

20. J. K. Bair and F. X. Haas, "Total Neutron Yield from the Reactions $^{13}C(\alpha,n)^{16}O$ and ^{17} $^{18}O(\alpha,n)^{20}$ ^{21}Ne," Phys. Rev. $\underline{C7}$, 1356 (1973).

21. J. K. Bair and H. B. Willard, "Level Structure in Ne^{22} and Si^{30} from the Reactions $O^{18}(\alpha,n)Ne^{21}$ and $Mg^{26}(\alpha,n)Si^{29}$," Phys. Rev. $\underline{128}$, 299 (1962).

22. J.K. Bair and J. Gomez del Campo, "Neutron Yields from Alpha-Particle Bombardment, Nucl. Sci. Eng. $\underline{71}$, 18 (1979).

23. Luisa F. Hansen, John D. Anderson, John W. McClure, Bertram A. Pohl, Marion L. Stelts, Jerome J. Wesolowski, and Calvin Wong, "The (α, ν) Cross Sections on ^{17}O and ^{18}O Between 5 and 12.5 MeV," Nucl. Phys. $\underline{A98}$, 25 (1967).

24. J. F. Ziegler, Helium Stopping Powers and Ranges in All Elemental Matter, Vol. 4 of The Stopping Ranges of Ions in Matter (Pergamon Press, New York, 1978).

25. L. C. Northcliffe and R. F. Schilling, "Range and Stopping Power Tables for Heavy Ions," Nuclear Data Tables $\underline{7}$, 233 (1970).

26. R. A. Friedenberg, "Construction of Isodose Contour Maps for the TFTR," Trans. Am. Nucl. Soc. $\underline{28}$, 657 (1978).

27. D. E. Bonnett, J. R. Williams, and C. J. Parnell, "The Isocentric Fast Neutron Therapy Facility at Edinburgh," British J. of Radiography $\underline{53}$, 12 (1979).

28. R. G. Alsmiller, Jr., T. A. Gabriel, and J. Barish, "Photon Dose Rate from Induced Activity in the Beam Stop of a 400 GeV Proton Accelerator," Nucl. Instrum. Methods $\underline{155}$, 399 (1978).

29. J. A. Holmes, S. E. Woosley, William A. Fowler, and B. A. Zimmerman, "Tables of Thermonuclear-Reaction-Rate Data for Neutron-Induced Reactions on Heavy Nuclei, At. Data and Nucl. Data Tables $\underline{18}$, 305 (1976).

30. S. E. Woosley, William A. Fowler, J. A. Holmes, and B. A. Zimmerman, "Semi-empirical Thermonuclear Reaction-Rate Data for Intermediate-Mass Nuclei," At. Data and Nucl. Data Tables $\underline{22}$, 371 (1978).

Page Range	Domestic Price	NTIS Price Code	Page Range	Domestic Price	NTIS Price Code	Page Range	Domestic Price	NTIS Price Code	Page Range	Domestic Price	NTIS Price Code
001-025	$ 5.00	A02	151-175	$11.00	A08	301-325	$17.00	A14	451-475	$23.00	A20
026-050	6.00	A03	176-200	12.00	A09	326-350	18.00	A15	476-500	24.00	A21
051-075	7.00	A04	201-225	13.00	A10	351-375	19.00	A16	501-525	25.00	A22
076-100	8.00	A05	226-250	14.00	A11	376-400	20.00	A17	526-550	26.00	A23
101-125	9.00	A06	251-275	15.00	A12	401-425	21.00	A18	551-575	27.00	A24
126-150	10.00	A07	276-300	16.00	A13	426-450	22.00	A19	576-600	28.00	A25
									601-up	†	A99

†Add $1.00 for each additional 25-page increment or portion thereof from 601 pages up.